ORIGINAL ARTICLE

CNS Neuroscience & Therapeutics   **WILEY**

Sleep waves in a large-scale corticothalamic model constrained by activities intrinsic to neocortical networks and single thalamic neurons

Martynas Dervinis | Vincenzo Crunelli ⓘ

Neuroscience Division, School of Bioscience, Cardiff University, Museum Avenue, Cardiff, CF10 3AX, UK

Correspondence
Martynas Dervinis and Vincenzo Crunelli, Neuroscience Division, School of Bioscience, Cardiff University, Museum Avenue, Cardiff CF10 3AX, UK.
Email: martynas.dervinis@gmail.com; crunelli@cardiff.ac.uk

Present address
Martynas Dervinis, School of Physiology, Pharmacology and Neuroscience, Biomedical Building, Bristol, BS8 1TD, UK

Abstract

Aim: Many biophysical and non-biophysical models have been able to reproduce the corticothalamic activities underlying different EEG sleep rhythms but none of them included the known ability of neocortical networks and single thalamic neurons to generate some of these waves intrinsically.

Methods: We built a large-scale corticothalamic model with a high fidelity in anatomical connectivity consisting of a single cortical column and first- and higher-order thalamic nuclei. The model is constrained by different neocortical excitatory and inhibitory neuronal populations eliciting slow (<1 Hz) oscillations and by thalamic neurons generating sleep waves when isolated from the neocortex.

Results: Our model faithfully reproduces all EEG sleep waves and the transition from a desynchronized EEG to spindles, slow (<1 Hz) oscillations, and delta waves by progressively increasing neuronal membrane hyperpolarization as it occurs in the intact brain. Moreover, our model shows that slow (<1 Hz) waves most often start in a small assembly of thalamocortical neurons though they can also originate in cortical layer 5. Moreover, the input of thalamocortical neurons increases the frequency of EEG slow (<1 Hz) waves compared to those generated by isolated cortical networks.

Conclusion: Our simulations challenge current mechanistic understanding of the temporal dynamics of sleep wave generation and suggest testable predictions.

KEYWORDS
biophysical model, delta waves, sleep spindles, slow (<1 Hz) waves, thalamic reticular nucleus

1 | INTRODUCTION

Recurrent activity in corticothalamic networks is key for the expression of EEG waves of natural sleep.[1–6] In particular, increases in neuronal membrane hyperpolarization resulting from the vigilance state-dependent, progressively decreasing firing of cholinergic, histaminergic, noradrenergic, and serotoninergic afferents from the hypothalamus and the brain stem underlies the transition from the

wake state to sleep spindles, delta, and slow (<1 Hz) waves.[7–10] To further our knowledge of the mechanisms underlying these EEG rhythms, many biophysical and non-biophysical models have been used to simulate sleep waves.[11–21] However, none of these models implemented the variety of neocortical neuron-specific sleep-related activities reported to occur in the isolated neocortex[22] and/or the ability of single thalamic neurons to elicit slow (<1 Hz) oscillations when isolated from the neocortex.[23–26]

Using current knowledge of anatomical connectivity,[27–37] we built a large-scale corticothalamic model that contains a single cortical column (with fast spiking, FS, inhibitory interneurons, and different excitatory neuronal populations) that is reciprocally connected to first-order and higher-order thalamic nuclei and its respective γ-aminobutyric acid (GABA)ergic neurons of the nucleus reticularis thalami (NRT). The model is constrained by implementing the ability of different neocortical populations to generate slow (<1 Hz) oscillations when detached from the thalamus[22,38] and single thalamic neurons to elicit sleep waves when isolated from the neocortex.[23–25]

Our corticothalamic model accurately reproduces all sleep EEG rhythms and the transition from a desynchronized EEG to various sleep rhythms. Our results show that the EEG slow (<1 Hz) waves are most often initiated by a small assembly of thalamocortical neurons though they can also originate in cortical layer 5 (L5) and that their frequency is decreased in the absence of thalamic afferent activity. Moreover, our simulations suggest testable predictions.

2 | METHODS

2.1 | Model architecture

The corticothalamic model contains 900 model neurons and is organized into six sectors (Figure S1): four cortical layers, including layers 2/3 (L2/3), 4 (L4), 5 (L5), and 6 (L6), and a first- and a higher-order thalamic nucleus with their thalamocortical neurons (TC$_{FO}$ and TC$_{HO}$, respectively) which are reciprocally connected to inhibitory NRT neurons (NRT$_{FO}$ and NRT$_{HO}$, respectively). Each cortical layer is divided in two subsectors, each with 100 excitatory and 50 inhibitory neurons. Cortical excitatory subsectors contain different number of regular spiking[39] (RS), intrinsically bursting[39,40] (IB), early firing[22] (EF), repetitive intrinsically bursting[22] (RIB), and network driver (ND) neurons,[22] whereas inhibitory subsectors have FS interneurons[41] (Figure S1). The full model is a two-dimensional stack of subsector neuron rows. The neuron position within a subsector was determined pseudo-randomly.

2.2 | Model network connectivity

The model network connectivity and the connection weights are provided in (Figure S1 and Tables S1,S2). Connections were organized topographically with sources and targets located in matching regions of their corresponding structures. A neuron did not synapse onto itself and could only form a single synapse on its target neuron. The number of contacts that a source neuron could form in a target structure was defined by the parameter P (a projection radius) (Table S1). Other key connectivity parameters (e.g., connection weight, postsynaptic potential shape, synaptic transmission latency, synaptic receptors) are listed in Table S2 and Supplementary Methods.

We made several simplifying assumptions. In certain instances, we scaled down differences in anatomical projection radii. This was

true for intra-cortical connections simplifying network calibration. Moreover, we scaled down the physiological N-methyl D-aspartate (NMDA) component in cortical synapses (i.e., 12–14 times smaller rather than three to five times as the AMPA component) in order to eliminate a slow periodicity component in paroxysmal simulations which had not been observed experimentally. NRT cells were connected by gap junctions,[42] that is, the first- and second-degree neighbors formed single 3 GΩ and 4.5 GΩ junctions, respectively.

2.3 | Model neurons

TC and NRT neurons were single-compartment Hodgkin–Huxley models whereas cortical neurons were Hodgkin–Huxley models with separate axosomatic and dendritic compartments. The equations for both thalamic and cortical neuron models are listed in the Supplementary Methods, that also describe the intrinsic and synaptic membrane currents and their dependence on intracellular ion concentration (where applicable) (Tables S3–S7).

2.4 | Simulations

All simulations were carried out in NEURON[43] on a desktop computer or one of the following computing clusters: the Neuroscience Gateway (NSG) Portal for Computational Neuroscience[44] or the Cardiff School of Biosciences Biocomputing Hub HPC/Cloud infrastructure.

2.5 | Data analysis

Simulation data were analyzed and visualized with the help of custom-written Matlab (MathWorks Inc routines). The scalp EEG signal produced by the simulations was estimated as described by Bédard et al (2004)[45] (see Supplementary Methods).

3 | RESULTS

First, we constrained the model by testing the ability of neocortical networks isolated from the thalamus to elicit slow (<1 Hz) oscillations and of single thalamic neurons to produce sleep spindles, delta waves, and slow (<1 Hz) oscillations, as reported in many in vitro studies.[22–25,38,46,47]

3.1 | Slow (<1 Hz) oscillations in the isolated neocortical network

We were able to reproduce the typical firing patterns observed at different levels of membrane polarization in RS and EF neurons, the pyramidal cell type that shows early firing during slow (<1 Hz)

oscillations[22] (Figure S2), as well as in IB and FS neurons[22] (Figure S3). We also developed models of RIB neurons and of the ND pyramidal neurons that "drive" slow (<1 Hz) oscillations in neocortical slices.[22] The firing patterns of RIB and ND neurons well matched those observed experimentally[22] (Figure S4A), including their input–output curves (Figure S4B).

When all these neocortical excitatory and inhibitory model neurons were synaptically connected in a cortical column (Figure S1), a pattern of non-rhythmic, low-amplitude activity was observed in the EEG for low K^{+} leak conductance (g_{KL}) values (Table S8) in all component neurons (Figure 1L,M). When g_{KL} was increased (Table S8), however, the neocortical network generated clear EEG slow (<1 Hz) waves (Figure 1C–E) that could also give rise to faster waves within the delta frequency band (Figure 1F–H). Thus, all neurons in all cortical layers oscillated at a frequency of 0.44 Hz (Figure 1C–E), that is, within the slow (<1 Hz) oscillation frequency, whereas at lower

g_{KL} values the oscillation reached the frequency of 1.57 Hz, that is, within the δ frequency range (Figure 1F–H): indeed, as g_{KL} was changed the neocortical oscillation frequency smoothly changed accordingly (not shown). Finally, further small progressive decreases in g_{KL} in all cortical cells (except EF neurons) (Table S8) resulted in the break-down of the regular pattern of oscillations (Figure 1I–K), and eventually led to a desynchronized, low-amplitude EEG similar to that of the wake state (Figure 1L,M) where single neurons fired randomly.

The slow (<1 Hz) oscillation elicited by the isolated neocortical network (Figure 1C–E) was initiated in L5 pyramidal neurons since the firing appeared there earlier than in other layers, followed by pyramidal neurons in L6, L2/3, and L4 (Figure S5A,B). In each layer, the inhibitory neuron firing occurred after that of the pyramidal neurons with little difference among layers (Figure S5A,B). The ND neurons in L5 are the cells that initiate the oscillation, followed by the
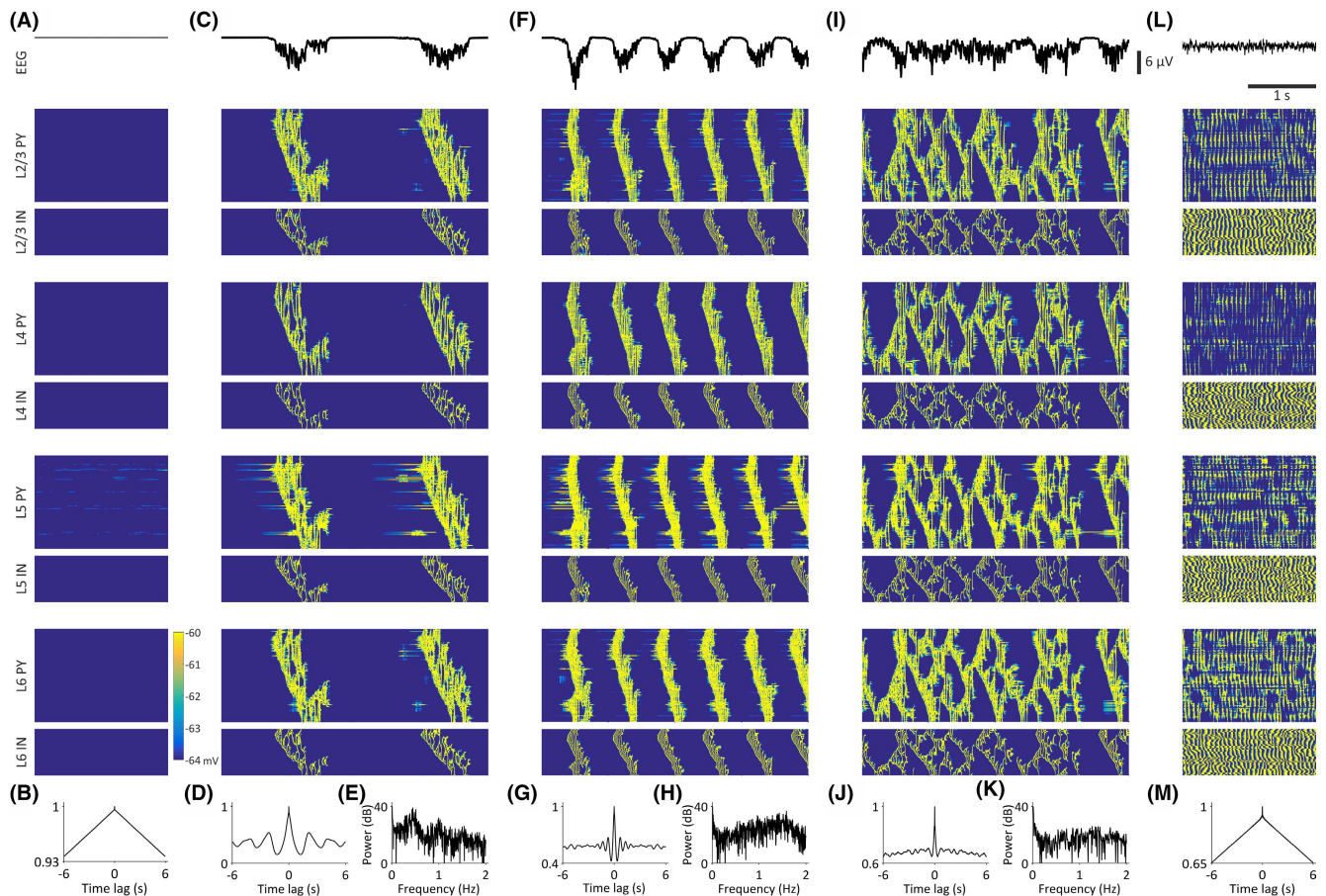

FIGURE 1 Slow (<1 Hz) and delta oscillations in the isolated neocortical model. EEG (top trace in A, C, F, I, L) and corresponding color-coded membrane potential graphs for the indicated neuronal populations (bottom traces in A, C, F, I, L), EEG autocorrelograms (B, D, G, J, M) and EEG power graphs (E, H, K) of the indicated activity. (A, B), with a large g_{KL} the cortical model does not elicit any activity. (C–E), Decreasing g_{KL} of ND and EF cells results in spontaneous slow (<1 Hz) oscillations in the entire cortical network. (F–H), Further reducing g_{KL} of ND cells leads to delta waves in the isolated cortical model. (I–K), When g_{KL} of other cortical neurons (except ND and EF neurons) is slightly decreased a non-regular activity pattern is observed, that is, there is a break-down of the oscillations. (L, M), The network shows a desynchronized EEG and tonic firing in all neuronal populations when g_{KL} of all cell types (except ND cells) is further decreased. L4 PY, pyramidal neurons in cortical layer 4; L4 IN, interneurons in cortical layer 4; L5 PY, pyramidal neurons in cortical layer 5; L5 IN, interneurons in cortical layer 5; L6 PY, pyramidal neurons in cortical layer 6; L6 IN, interneurons in cortical layer 6; L2/3 PY, pyramidal neurons in cortical layers 2 and 3; L2/3 IN, interneurons in cortical layers 2 and 3.

EF neurons in L/6 and L2/3 (Figure S5C). Thus, the onset timing of the simulated neocortical slow (<1 Hz) oscillation is highly consistent with experimental data obtained in cortical slices.[22,38] Indeed, the duration of the up- and down-states of the simulated slow (<1 Hz) oscillations in the isolated neocortex was similar to that observed in vitro (~250 ms and ~840 ms, respectively)[22] (Figure S5D,E).

The two main contributors to the maintenance of the up-state were, in order of importance, the persistent Na^+ current ($I_{Na(P)}$) and the excitatory postsynaptic potential (EPSP) barrage in IB (Figures S6D,F) and RS (not shown) neurons. Reducing α-amino-3-hydroxy-5-methyl-4-isoxazolepropionic acid (AMPA)-mediated EPSPs or $I_{Na(P)}$ abolished up-states (Figure S7B,F) confirming their causal roles in the initiation and maintenance of the slow (<1 Hz) oscillation, whereas blockade of NMDA receptors had little impact on up-states, indicating that NMDA receptor function is not necessary for the maintenance of cortical up-states (Figure S7C).

Other significant contributors in maintaining the up- and down-state dynamics were the A-type K^+ current (I_A) and the inhibitory postsynaptic potential (IPSP) barrage (Figures S6F and S7G). Their blockade resulted in over-excitation and the transformation of the slow (<1 Hz) oscillation into a paroxysmal oscillation (Figures S7D) (implying a balancing role for $GABA_A$ receptors) or in the disappearance of the down-states as the remaining K^+ currents could no longer terminate up-states (Figure S7G) (implying a role for I_A in the termination of the slow (<1 Hz) oscillation). The total intrinsic hyperpolarizing and depolarizing currents were similar as were the excitatory and inhibitory synaptic currents (Figure S6D,E,I).

The termination of the up-state occurred because of the gradual accumulation of the Ca^{2+}-activated K^+ current ($I_{K[Ca]}$) but also the M-type K^+ current (I_M) and the Na^+-activated K^+ current ($I_{K[Na]}$) (Figure S6G). Blocking $I_{K[Ca]}$ in all model neurons except ND increased the up-state duration confirming its causal role in the termination (Figure S7I). Similarly, block of I_M increased the duration and irregularity of the up-states confirming its role in curtailing up-states (Figure S7J). On the other hand, the block of $I_{K[Na]}$ resulted in an almost-continuous up-state, that is, the up-state never properly terminated (Figure S7K) since EF neurons fired continuously (not shown).

The contribution to the initiation, maintenance, and termination of up-states by the T-type Ca^{2+} current (I_T), the high-threshold Ca^{2+} current (I_{HVA}), and the hyperpolarization-activated, cyclic nucleotide-gated current (I_h) was negligible in IB and RS model cells (Figure S6H). Blocking I_T, I_{HVA}, and I_h (except for ND) had no significant effect on

the duration or shape of the up-states (Figure S7L–N). However, I_h and I_{HVA}, as the key pacemaker currents, initiated the up-states in ND neurons (not shown).

Blocking $GABA_A$Rs resulted in a continuous paroxysmal oscillation (Figure S7D) as it was observed experimentally in cortical slices after application of bicuculline.[48] Hence, the effect of $GABA_A$Rs is to reduce the intensity of cortical up-states and, in turn, to increase their duration by limiting the build-up of $I_{K[Ca]}$ and $I_{K[Na]}$, an observation consistent with the experimental data.[49] The role of $GABA_B$Rs was to shorten the up-states since their blockade resulted in up-states longer than 1 s (Figure S6E), an effect opposite to that of $GABA_A$R and consistent with in vitro experiments.[49]

Having established the dynamics of initiation and maintenance of the EEG slow (<1 Hz) oscillation in the isolated cortical network, we next investigated whether the membrane potential waveforms of the different cortical populations during the up- and down-states dynamics were similar to those observed in neocortical slices.[22,38] The excitatory RS, EF, and ND neurons faithfully reproduced the up- and down-state dynamics, the firing patterns, and the bimodal distribution of the membrane potential characteristic of neocortical slow (<1 Hz) oscillations in vitro[22] (Figure 2A–H, M–P). In particular, ND neurons exhibited the diverse activity observed in this pyramidal neuron type at an early and late stages of the slow (<1 Hz) oscillation as shown following its pharmacological induction in cortical slices[22] (Figure 2O,P). Moreover, the membrane potential waveform of IB and RIB pyramidal neuron models during the simulated neocortical slow (<1 Hz) oscillations well matched that reported in cortical slices[22] (Figure S8). A slow (<1 Hz) oscillation was also present in the inhibitory FS neurons, although a clear bimodal distribution was evident in their firing but not in their membrane potential distribution plots as observed experimentally[22] (Figure 2I–L). Finally, a faithful reproduction of the slow (<1 Hz) oscillation and its membrane potential distribution plots was also found for IB and RIB neurons[22] (Figure S8).

3.2 | Intrinsic slow (<1 Hz) oscillations of thalamic neurons

Our model TC_{FO}, TC_{HO}, NRT_{FO}, and NRT_{HO} neurons reproduced the 'classical' activity patterns of these cells, that is, tonic single action potential (AP) and T-type Ca^{2+} channel-mediated burst firing, in particular the typical burst signature of decelerando and

FIGURE 2 Experimental and simulated membrane potential dynamics in cortical neurons during slow (<1 Hz) oscillations in the isolated cortical network. (A, B), Simultaneous local field potential and membrane potential dynamics of an RS neuron recorded in vitro (experiment) during slow (<1 Hz) oscillations and its simulated activity in the isolated cortical network (simulation). The left-hand traces show the initial stage of the oscillation while the right-hand traces show the oscillation at a later stage (increased neuromodulatory drive). (C, D), Normalized membrane potential distribution plots for the experimental and simulated slow (<1 Hz) oscillations of an RS neuron with the typical peaks of the up- and down-states. (E, F), Same as (C, D) but for an EF neuron. (G, H), Same as (A, B) for an EF neuron. (I, J), Same as (A, B) but for an FS neuron. (K, L), Same as (C, D) but for an FS neuron. Note the lack of a clear bimodal membrane potential distribution in the plots of both the experimental and simulated data of the FS neurons. (M, N), Same as (C, D) but for an ND neuron. (O, P), Same as (A, B) but for an ND neuron. Experimental data are reproduced with permission from Lorincz et al. (2015).[22]

(A) RS experiment
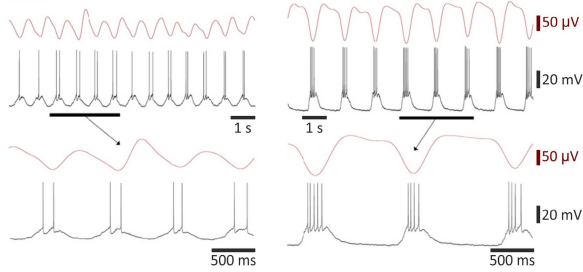
(B) RS simulation
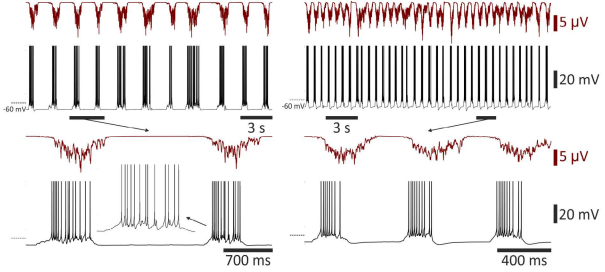
(C) RS experiment
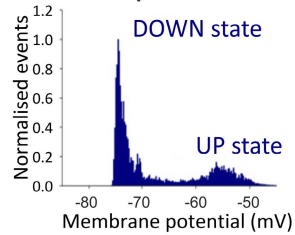
(D) RS simulation
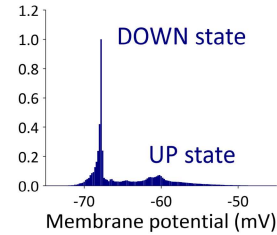
(E) EF experiment
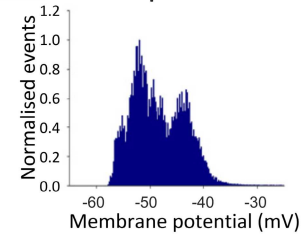
(F) EF simulation
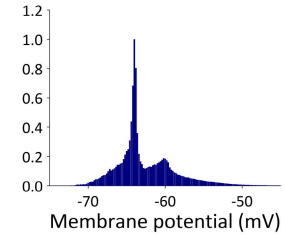
(G) EF experiment
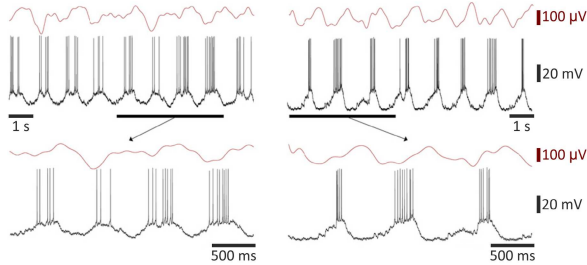
(H) EF simulation
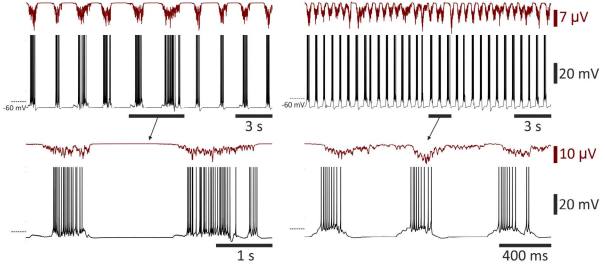
(I) FS experiment
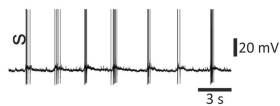
(J) FS simulation
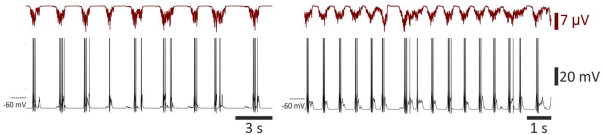
(K) FS experiment
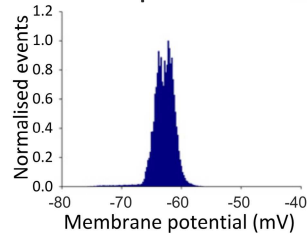
(L) FS simulation
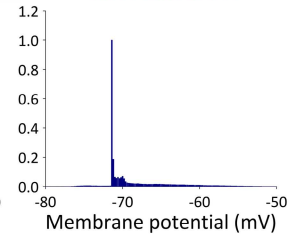
(M) ND experiment
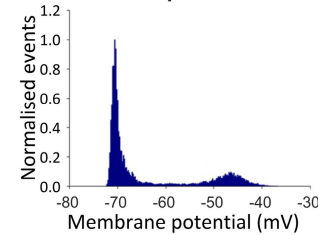
(N) ND simulation
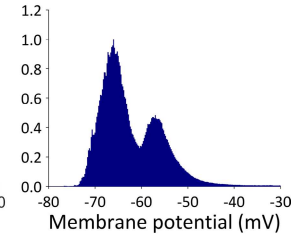
(O) ND experiment
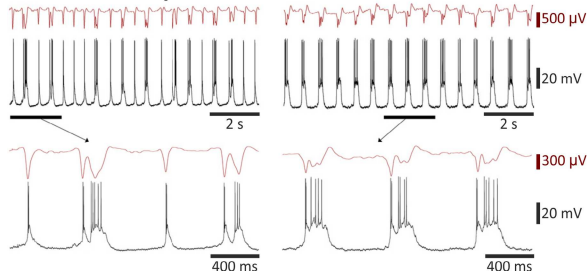
(P) ND simulation
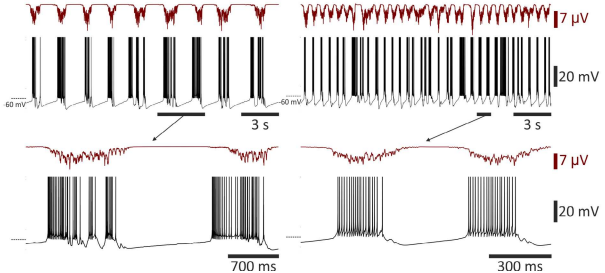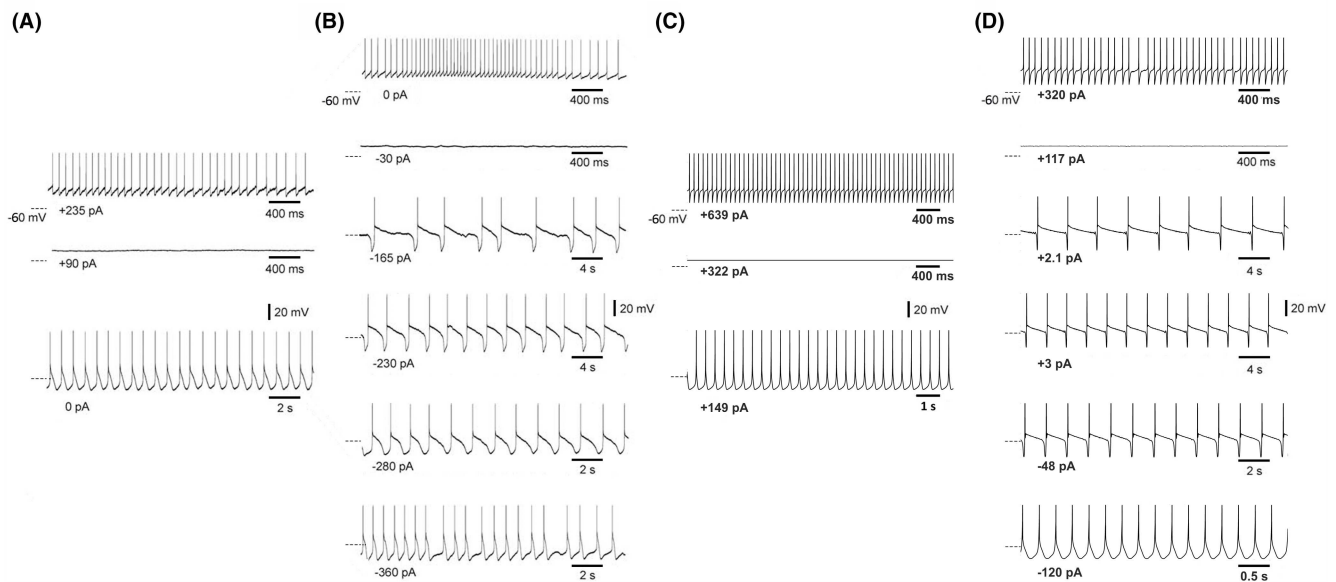
Experiment   Simulation

FIGURE 3 Experimental and simulated membrane potential dynamics of TC_FO neurons during intrinsically generated slow (<1 Hz) oscillations. (A), Tonic firing (top trace), quiescence (middle trace), and delta oscillations (bottom trace) are observed at different level of membrane polarization (injected current at the bottom of each trace) in a cat ventrobasal TC neuron recorded in a thalamic slice maintained in a standard recording solution. (B), After application of 100 μM trans-ACPD (a metabotropic glutamate receptor, mGluR, agonist) the same neuron shows slow (<1 Hz) oscillations between the quiescent state and the delta oscillations (bottom trace). (C), Simulation in the TC_FO neuron model of the experimental activity shown in (A). (D), Simulation of experimental activity shown in (B) was obtained after reducing g_{KL} of the TC_FO neuron model to mimic the effect of mGluR activation in vitro. Dashed lines on the left of each trace indicate −60 mV. (A) and (B) are reproduced with permission from Zhu et al. (2006).[25]

accelerando–decelerando burst firing patterns of TC and NRT neurons,[50] respectively (not shown).

We then simulated the intrinsic generation of delta and slow (<1 Hz) oscillations observed in TC_FO neurons in vitro following pharmacological activation of metabotropic glutamate receptors 1a (mGluR1a),[23–25] which was mimicked by reducing g_{KL} (Figure 3). The TC_FO neurons closely reproduced the hyperpolarization-dependent transition from tonic firing to slow (<1 Hz) oscillations at increasing frequency (due to shorter up states) and then to delta waves (Figure 3B,D). Moreover, the full spectrum of delta and slow (<1 Hz) oscillations observed at different levels of membrane polarization

were elicited by the NRT_FO neuron model (Figures S9). Notably, $I_{Na(P)}$ and the Ca^{2+}-activated non-specific cation current (I_{CAN}) played a major role in the duration of the up-state of NRT_FO neurons since their reduction led to a progressive shortening, and eventually to the abolition of, the up-states, that is, the slow (<1 Hz) oscillation was gradually transformed into a delta wave (Figure S10B1–C2). Notably, NRT_FO neurons were capable of eliciting both slow and fast sleep spindle waves (6.5–16 Hz) in isolation, that is, when disconnected from TC_FO neurons (Figure S11). Finally, TC_HO and NRT_HO neurons reproduced slow (<1 Hz) and delta oscillations similar to those of TC_FO and NRT_FO neurons, respectively (not shown).

FIGURE 4 Slow (<1 Hz) oscillations in the full corticothalamic model. (A), EEG showing the rhythmic pattern of slow (<1 Hz) oscillations. (B), EEG (top trace) and color-coded membrane potential plots of the indicated cortical and thalamic neuronal populations during the five cycles of the slow (<1 Hz) oscillation highlighted in (A) (note the two separate color-scales for the cortical and thalamic neurons). Below are the corresponding membrane potential waveforms of the two neurons indicated by the red arrow on the left of the corresponding color-coded plots. (C), EEG (top trace), AP rastergrams of the firing in each neuronal population for the slow (<1 Hz) oscillation cycle highlighted in (B). Red dashed vertical line represents the first AP of the up-state in each population. The latency (indicated in red below each rastergram) is measured relatively to the first AP of the cycle in the TC_FO neuron that fires first (time zero). Below the rastergrams are the corresponding membrane potential waveforms of that cycle for the indicated neuron. (D), Cross-correlations of EEG and membrane potential (black trace) and EEG and APs (color trace) for the indicated neuronal populations, calculated over a 485 s-long simulation. Shaded regions are 95% confidence intervals. (E), Enlargement of the highlighted sections of the membrane potential color plot of the TC_FO neurons. L4 FS, FS neuron in cortical layer 4; L4 IB, IB neuron in cortical layer 4; L4 IN, interneurons in cortical layer 4; L4 PY, pyramidal neurons in cortical layer 4; L5 FS, FS neuron in cortical layer 5; L5 IN, interneurons in cortical layer 5; L5 PY, pyramidal neurons in cortical layer 5; L5 RS, RS neuron in cortical layer 5; NRT_FO, first-order NRT neurons; NRT_HO, higher-order NRT neurons; TC_FO, first-order TC neurons; TC_HO, higher-order TC neurons.
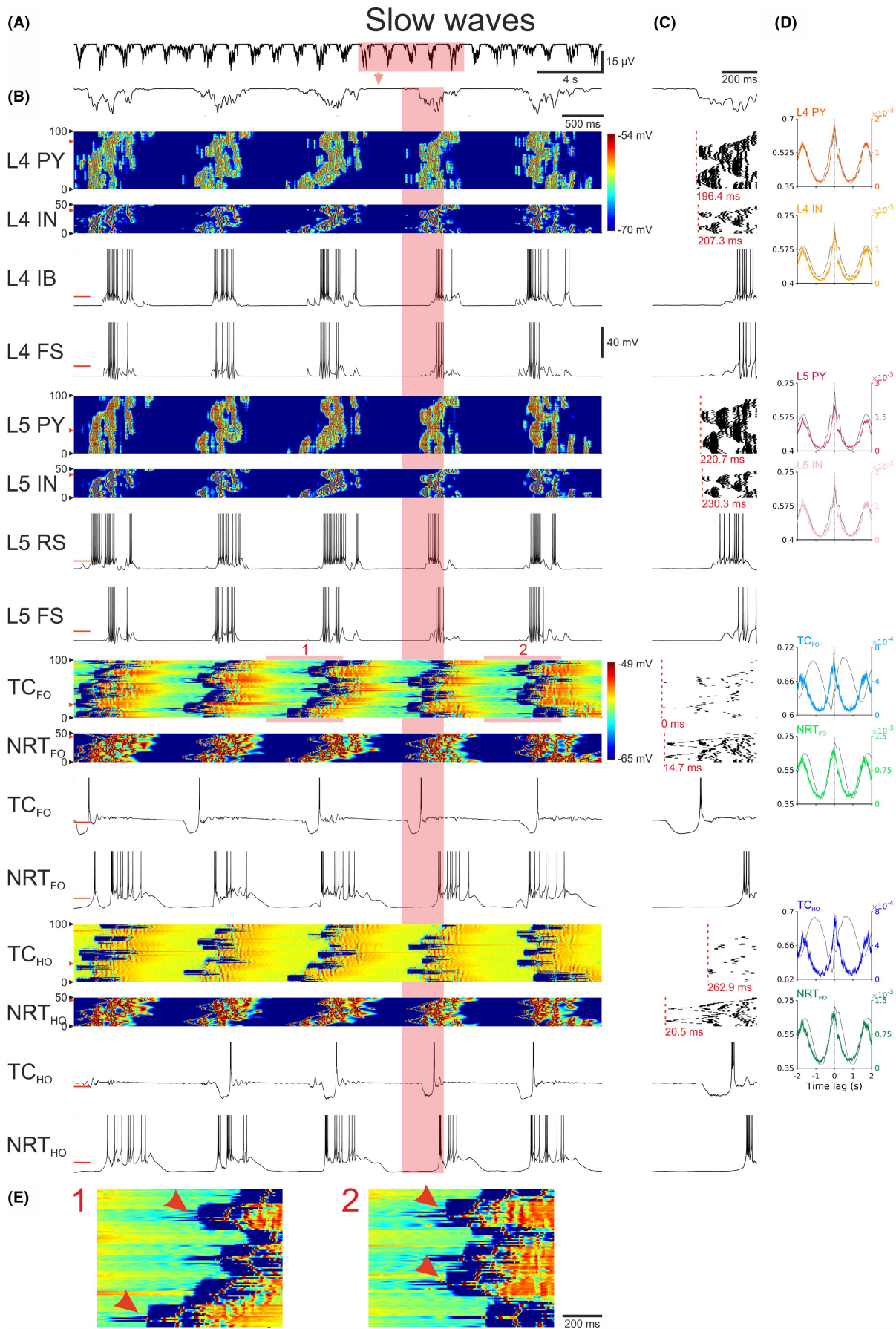
3.3 | Sleep waves in the full corticothalamic model

Experimentally it was shown that whereas the neocortex can generate the slow (<1 Hz) oscillation when isolated from the thalamus, its up-states are less rhythmic and frequent in the absence of the thalamus,[52] a finding that was faithfully reproduced by our full corticothalamic model (Figure S12). Connecting cortex and thalamus produced stronger up-state firing in both structures: as a result, K$^+$ currents accumulated faster and the up-states terminated earlier in both structures (not shown). Having shorter thalamic up-states shortened the whole oscillation cycle because the duration of thalamic down-states changed little since they are mostly controlled by intrinsic currents. As a result, the next global oscillation cycle was brought forward by an early onset of I$_T$-mediated burst firing of TC$_{FO}$ neurons which initiated the up-states in the cortical neurons (Figure S12).

Figure 4A shows simulated slow (<1 Hz) oscillation in the full corticothalamic model with up-states occurring with a regular periodicity across all neuronal populations. Most commonly (see the first four up-states in Figure 4B), the up-state-linked firing appeared initially in a small number of TC$_{FO}$ neurons that, notably, was different from one up-state to the next (Figure 4B,C). This was followed by firing in NRT$_{FO}$ and NRT$_{HO}$ neurons and then in L4, L5, L6, and L2/3, with the start of the EEG slow wave coinciding with the start of the L4 neuron firing (Figure 4C). Notably, when ND cells were depolarized, up-states could also start in L5 (Figure S13). TC$_{HO}$ neurons only started firing after all cortical neurons, indicating that cortically driven excitation, more than early inhibition from NRT$_{HO}$ neurons, was necessary to elicit rebound firing at the start of the up-states in these thalamic neurons (Figure 4C), as shown experimentally.[23–25]

The membrane potential waveforms of different neuronal types during the slow (<1 Hz) oscillation were similar to those observed experimentally in vivo[1,46,52] (Figure 4B). The most active up-states (i.e., containing APs) among the cortical neurons were in ND, EF, and FS neurons, whereas RS, IB, and RIB displayed on average a sparser firing (Figure 4B). The firing in thalamic neurons was more regular than in cortex and had a clear intrinsic aspect to it (Figure 4B). The onset of regularly shaped up-states in all thalamic neurons followed a down-state of an almost fixed length and invariably terminated

with an I$_T$-mediated burst of action potentials (Figures 3D and 4A), as observed in thalamic neurons in vitro[23–26]: indeed, thalamic activity was essentially an intrinsic oscillation that was shaped by, and synchronized with, the neocortex, a result supported by experimental findings.[26,53]

Notably, when g$_{KL}$ of TC and NRT neurons was increased (Table S9) delta waves started to occur during the down-states of the slow (<1 Hz) oscillations of these thalamic neurons, as observed experimentally[23–25]: their reflection in the cortical territory resulted in a speeding up of the slow (<1 Hz) oscillation into the delta frequency range (Figure 5B) as seen in the EEG (Figure 5A). Whereas during slow (<1 Hz) waves firing was observed first in a small number of TC$_{FO}$ neurons, during delta waves there was little time lag across the entire TC$_{FO}$ neuron population and the delay between thalamic and L4 neuron firing in each cycle was much smaller (<100 msec) (Figure 5C–F).

Finally, by adjusting g$_{KL}$ and increasing the fast component of K$^+$ after hyperpolarizing current (I$_{AHP}$) in NRT cells the corticothalamic model was able to reproduce EEG sleep spindles (Figures 6 and S14). Spindle waves appeared regularly in the EEG and had the "classical" waveform observed in vivo[1,46] (Figures 6A,B and S14A,B). During a spindle wave, firing started in NRT$_{FO}$ neurons, followed in a few milliseconds by TC$_{HO}$ and NRT$_{HO}$ neurons, and then TC$_{FO}$ and cortical neurons (Figure 6B–E). Notably, the first firing in TC$_{FO}$ neurons resulted from IPSPs summation leading to a rebound burst, partly explaining the firing initiation in these thalamic neurons (Figure 6B,E). However, the first firing of a spindle cycle could also originate in TC$_{HO}$ neurons (Figure S14). Notably, in both cases it is evident that the spindle wave builds up in the thalamus before being reflected into the cortical territory (Figures 6C and S14B).

4 | DISCUSSION

The main finding of this study, that used a bottom-up modeling strategy to constrain the corticothalamic model with parameters obtained from in vivo and in vitro experiments, is the ability to replicate in the EEG and in cortical and thalamic neuronal populations the slow (<1 Hz), delta, and spindle waves and the transition between these

FIGURE 5 Delta waves in the full corticothalamic model. (A), EEG showing a period of rhythmic delta waves. (B), EEG (top trace) and color-coded membrane potential plots of the indicated cortical and thalamic neuronal populations during the section of delta waves highlighted in (A) (note the two separate color-scales for the cortical and thalamic neurons). Below are the corresponding membrane potential waveforms of the two neurons indicated by the red arrow on the left of the corresponding color-coded plots. (C), EEG (top trace), AP rastergrams of the firing of each neuronal population for the delta wave cycle highlighted in (B). Red dashed vertical line represents the first AP of the up-state in each population. The latency (indicated in red below each rastergram) is measured relatively to the first AP of the cycle in the TC$_{FO}$ neuron that the fires first (time zero). Below the rastergrams are the corresponding membrane potential waveforms of that cycle for the indicated neuron. (D), Cross-correlations of EEG and membrane potential (black trace) and EEG and APs (color trace) for the indicated neuronal populations, calculated over a 485 s-long simulation. Shaded regions are 95% confidence intervals. Dashed vertical line indicates zero lag. (E), Distribution of the first AP in a delta wave cycle with respect to the EEG for all APs of the indicated neuronal populations. Shaded regions are 95% confidence intervals. Dashed vertical line indicates zero lag. L4 FS, FS neuron in cortical layer 4; L4 IN, interneurons in cortical layer 4; L4 PY, pyramidal neurons in cortical layer 4; L4 RS, RS neuron in cortical layer 4; L5 FS, FS neuron in cortical layer 5; L5 IB, IB neuron in cortical layer 5; L5 IN, interneurons in cortical layer 5; L5 PY, pyramidal neurons in cortical layer 5; NRT$_{FO}$, first-order NRT neurons; NRT$_{HO}$, higher-order NRT neurons; TC$_{FO}$, first-order TC neurons; TC$_{HO}$, higher-order TC neurons.
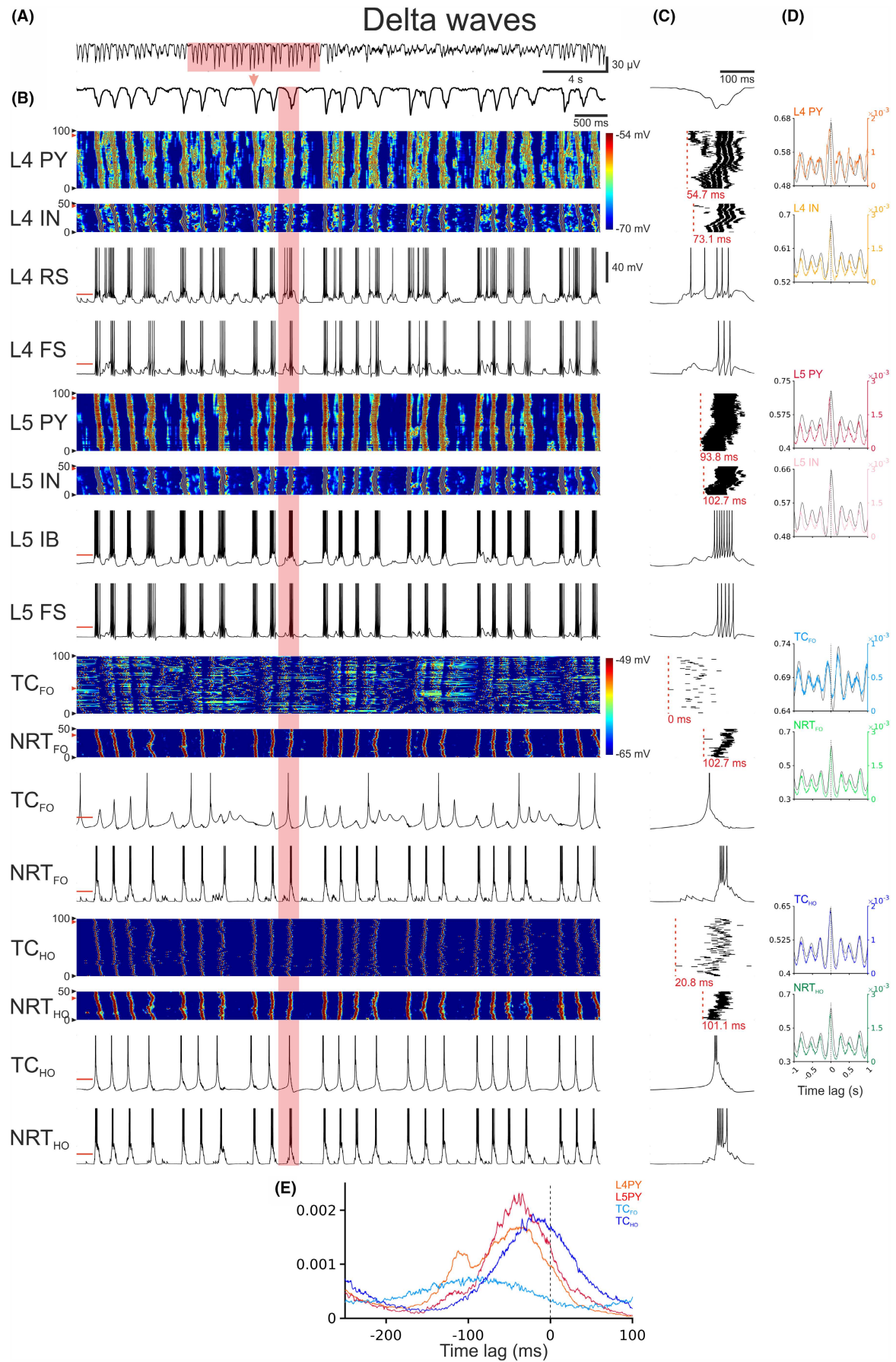
sleep states by mimicking the neuronal input resistance changes induced by the hypothalamic and brain stem neuromodulatory drives. Indeed, our simulation results remarkably well reproduced the neuronal firing patterns and their sequence of occurrence during different sleep waves, the membrane potential bistability underlying the slow (<1 Hz) oscillation in single cortical and thalamic neurons, the onset and duration dynamics of up- and down-states, and the increased regularity and frequency imposed by the thalamus on the slow (<1 Hz) oscillation of the isolated neocortical network.

4.1 | Model limitations

The ND neuron model has limitations, including the down-states being more depolarized and having a larger variance due to a pronounced I_h-mediated sag than ND neurons recorded in vitro.[22] It may be possible that I_T is the main pacemaker in the real ND neurons as opposed to I_{HVA} in the model cells. In the absence of experimental data, initial attempts to model ND neurons used the I_T of TC neurons. However, either because I_T parameters are not appropriate for the cortical axosomatic and dendritic compartments or the model ND neuron morphology was inadequate, I_T did not support the intrinsic slow (<1 Hz) oscillation. Having I_T as the actual pacemaker current and not I_{HVA} could drastically stabilize slow (<1 Hz) oscillations by increasing the membrane potential difference between up- and down-states in ND neurons and by increasing the AP frequency within a burst leading to more densely packed EPSPs in the postsynaptic neurons and thus helping the transition to a new up-state.

The frequency of slow/delta intrinsic oscillations of ND cells increases as they are more depolarized, a result similar to that observed in vitro[22] This, in turn, is reflected in the frequency of modeled cortical network slow/delta oscillations, although this is the opposite of the results in cortical slices.[22] As indicated above, this is most likely the consequence of the lack of any data on the relative contribution of different intrinsic currents to the excitability of these neurons.

The model does not include the tight regulation of the intrinsic oscillations of thalamic neurons by changes in the function of their metabotropic glutamate receptors as shown experimentally,[23–25]

that is, the ability of these neurons to behave as conditional oscillators.[26] This could be achieved by linking activation of these modulatory receptors to the firing of the thalamic projecting L5-6 axons, as shown with electrical stimulation of the corticothalamic afferents in thalamic slices.[54]

4.2 | Model strengths

Up-states in the cortical network model were initiated by ND and EF neurons, and, to the best of our knowledge, this study is the first that successfully simulate EEG slow (<1 Hz) waves with these intrinsic mechanisms. However, having these intrinsic initiation processes does not exclude the involvement of other mechanisms of initiation and maintenance of this sleep rhythm, in particular the accumulation of spontaneous synaptic activity[55] and the synchronization of already active neuronal assemblies.[56] Notably, however, in our model simulated excitatory synaptic conductances were slightly higher than the inhibitory ones, in contrast to experimental studies that reported the opposite[57] or an equal influence by the two,[58] although these studies were performed in vitro.

Thus, our model confirms and enlarges our previous simulations obtained in a thalamocortical model with a limited number of cortical neuron types and fewer thalamic neuron conductances.[19] Notably, our simulations are also in agreement with the experimental data of David et al. (2013)[51] as they show that connecting thalamus to cortex increases the frequency and rhythmicity of EEG slow (<1 Hz) waves.

Whereas in the isolated neocortex, the appearance of the slow (<1 Hz) oscillations matches the temporal profile reported in cortical slices,[22,38] that is, L5, and L4 and L6, in the full corticothalamic model the first *cortical* firing is preferentially observed in L4 followed by L5 and then L6. This is not surprising because of the prevailing input to L4 from the TC_{FO} neurons that are the first to start firing in the full corticothalamic model. However, there are cases in the corticothalamic model where firing starts in L5, as in neocortical slices.[22,38] Thus, whereas the full corticothalamic model maintains the inherent ability of cortical networks to start slow (<1 Hz) oscillations in L5, the thalamocortical input most often prevails when the reciprocal

FIGURE 6 Sleep spindles in the full corticothalamic model. (A), EEG showing the rhythmic pattern of sleep spindles. (B), EEG (top trace) and color-coded membrane potential plots of the indicated cortical and thalamic neuron populations during the sleep spindle highlighted in (A) (note the two separate color-coded scales for the cortex and the thalamus). Below are the corresponding membrane potential waveforms of the two neurons indicated by the red arrow on the left of the corresponding color-coded plots. (C), EEG (top trace), AP rastergrams of the firing of the first AP in each neuronal population for the onset of sleep spindles highlighted in (B). Red dashed vertical line represents the first AP of the up-state in each population. The latency (indicated below each rastergram) is measured relatively to the first AP of the cycle in an NRT_{FO} neuron (time zero). Below the rastergrams are the corresponding membrane potential waveforms of that cycle for the indicated neuron. (D), Cross-correlations of EEG and membrane potential (black trace) and EEG and APs (color trace) for the indicated neuronal populations, calculated over a 485 s-long simulation. Shaded regions are 95% confidence intervals. Dashed vertical line indicates the zero lag. (E), AP distribution with respect to the EEG for all APs of the indicated neuronal populations. Shaded regions are 95% confidence intervals. Dashed vertical line indicates the zero lag. L4 FS, FS neuron in cortical layer 4; L4 IB, IB neuron in cortical layer 4; L4 IN, interneurons in cortical layer 4; L4 PY, pyramidal neurons in cortical layer 4; L5 FS, FS neuron in cortical layer 5; L5 IN, interneurons in cortical layer 5; L5 PY, pyramidal neurons in cortical layer 5; L5 RS, RS neuron in cortical layer 5; NRT_{FO}, first-order NRT neurons; NRT_{HO}, higher-order NRT neurons; TC_{FO}, first-order TC neurons; TC_{HO}, higher-order TC neurons.
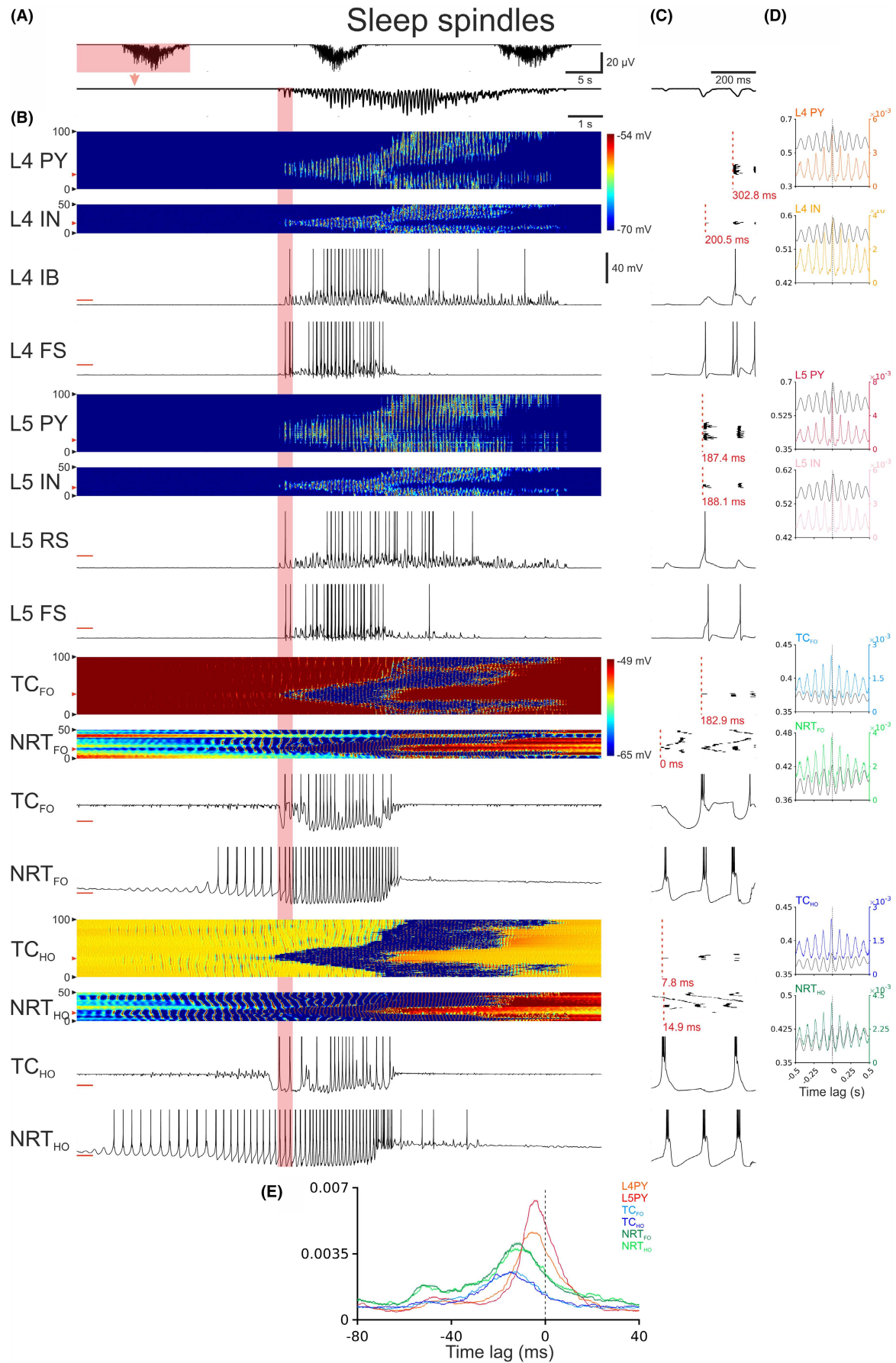
cortical and thalamic projection are active. Indeed, a recent study in humans indicates that slow (<1 Hz) oscillations in the anterior thalamus precede those in neocortical territories.[59]

Finally, connecting thalamus and cortex allows the simultaneous occurrence of different sleep rhythms. In fact, our simulations show that whereas the isolated cortex is capable of generating slow (<1 Hz) and delta oscillations they cannot occur at the same time. In contrast, when the thalamocortical input is intact, slight changes in g_{KL} could smoothly increase the frequency of slow (<1 Hz) oscillations (with a progressive decrease in the up-state duration), eventually leading to delta waves where as shown experimentally[23–25] the low threshold calcium potential does not lead to an up-state, that is, there is a continuum between slow (<1 Hz) and delta oscillations. Also, sequences of sleep spindles start being expressed cortically and are typically grouped by up-states. In summary, the richness and versatility of oscillatory behaviors displayed by the full corticothalamic model is, as expected, far greater than any of those generated by its constituent parts, that is, neocortex and thalamus, in isolation.

4.3 | Predictions and future studies

Our simulation results suggest testable predictions that should guide future studies. These may include:

1. temporal dynamics of cortical firing during sleep slow (<1 Hz) waves in non-anesthetized humans and in naturally waking–sleeping animals;
2. relative contribution of $I_{Na(P)}$ and I_{CAN} to the intrinsic slow (<1 Hz) oscillations of TC and NRT neurons;
3. currents essential to slow (<1 Hz) oscillations in TC and NRT neurons, in particular $I_{Twindow}$, although the large dendritic distribution of I_T[60,61] may render this work difficult;
4. re-investigation of the ability of NRT neurons to generate intrinsically sleep spindles in freely moving animals with combined optogenetic and large neuronal assembly recordings and in thalamic slice where the hypothalamic and brain stem drives, known to modulate I_{AHP},[10] are artificially recreated;
5. the pacemaker currents of neocortical neurons, in particular I_T, I_{HVA}, and I_h, in ND and EF neurons;
6. relative contribution of $I_{Na(P)}$, $I_{K[Na]}$, and other intrinsic currents to initiation, maintenance, and termination of up-states in the isolated cortex;
7. increased frequency of corticothalamic slow (<1 Hz) oscillation up-states (due to the presence of the thalamic drive) compared to those generated by the isolated cortical network;
8. corticothalamic sleep spindle generation by combination of input resistance and neuromodulators-dependent changes in I_{AHP} of NRT neurons.

AUTHORS' CONTRIBUTION

The model codes are available to download from Github via Zenodo (https://doi.org/10.5281/zenodo.7724411 and https://doi.org/10.5281/zenodo.7724443).

ORCID

Vincenzo Crunelli https://orcid.org/0000-0001-7154-9752

REFERENCES

1. Contreras D, Steriade M. Spindle oscillation in cats: the role of corticothalamic feedback in a thalamically generated rhythm. *J Physiol*. 1996;490:159-179.
2. Destexhe A, Contreras D, Steriade M. Spatiotemporal analysis of local field potentials and unit discharges in cat cerebral cortex during natural wake and sleep states. *J Neurosci*. 1999;19:4595-4608.
3. Steriade M, Timofeev I, Grenier F. Natural waking and sleep states: a view from inside neocortical neurons. *J Neurophysiol*. 2001;85:1969-1985.
4. Dang-Vu TT, Schabus M, Desseilles M, et al. Spontaneous neural activity during human slow wave sleep. *Proc Natl Acad Sci USA*. 2008;105:15160-15165.
5. Vyazovskiy V, Olcese U, Lazimy YM, et al. Cortical firing and sleep homeostasis. *Neuron*. 2009;63:865-878.
6. von Ellenrieder N, Gotman J, Zelmann R, et al. How the human brain sleeps: direct cortical recordings of Normal brain activity. *Ann Neurol*. 2020;87:289-301.
7. Osorio-Forero A, Cardis R, Vantomme G, et al. Noradrenergic circuit control of non-REM sleep substates. *Curr Biol*. 2021;31:5009-5023.
8. Nghiem TE, Tort-Colet N, Górski T, et al. Cholinergic switch between two types of slow waves in cerebral cortex. *Cereb Cortex*. 2020;30:3451-3466.
9. Brown RE, Basheer R, JT MK, Strecker RE, RW MC. Control of sleep and wakefulness. *Physiol Rev*. 2012;92:1087-1187.
10. McCormick DA. Neurotransmitter actions in the thalamus and cerebral cortex and their role in neuromodulation of thalamocortical activity. *Prog Neurobiol*. 1992;39:337-388.
11. Tóth T, Crunelli V. Computer simulation of the pacemaker oscillations of thalamocortical cells. *Neuroreport*. 1992;3:65-68.
12. Destexhe A, Bal T, McCormick DA, Sejnowski TJ. Ionic mechanisms underlying synchronized oscillations and propagating waves in a model of ferret thalamic slices. *J Neurophysiol*. 1996;l76:2049-2070.
13. Bazhenov M, Timofeev I, Steriade M, Sejnowski TJ. Model of thalamocortical slow-wave sleep oscillations and transitions to activated states. *J Neurosci*. 2002;22:8691-8704.
14. Compte A, Sanchez-Vives MV, McCormick DA, Wang XJ. Cellular and network mechanisms of slow oscillatory activity (<1 Hz) and wave propagations in a cortical network model. *J Neurophysiol*. 2003;89:2707-2725.
15. Hill S, Tononi G. Modeling sleep and wakefulness in the thalamocortical system. *J Neurophysiol*. 2005;93:1671-1698.
16. Traub RD, Contreras D, Cunningham MO, et al. Single-column thalamocortical network model exhibiting gamma oscillations, sleep spindles, and epileptogenic bursts. *J Neurophysiol*. 2005;93:2194-2232.

17. Destexhe A. Self-sustained asynchronous irregular states and up-down states in thalamic, cortical and thalamocortical networks of nonlinear integrate-and-fire neurons. *J Comput Neurosci.* 2009;27:493-506.

18. Bazhenov M, Lonjers P, Skorheim S, Bedard C, Dstexhe A. Non-homogeneous extracellular resistivity affects the current-source density profiles of up-down state oscillations. *Philos Trans A Math Phys Eng Sci.* 2011;369:3802-3819.

19. Crunelli V, Errington AC, Hughes SW, Tóth TI. The thalamic low-threshold Ca^{2+} potential: a key determinant of the local and global dynamics of the slow (<1 Hz) sleep oscillation in thalamocortical networks. *Philos Trans A Math Phys Eng Sci.* 2011;369:3820-3839.

20. Bonjean M, Baker T, Bazhenov M, Cash S, Halgren E, Sejnowski T. Interactions between core and matrix thalamocortical projections in human sleep spindle synchronization. *J Neurosci.* 2012;32:5250-5263.

21. Rosen BQ, Krishnan GP, Sanda P, et al. Simulating human sleep spindle MEG and EEG from ion channel and circuit level dynamics. *J Neurosci Methods.* 2019;316:46-57.

22. Lőrincz ML, Gunner D, Bao Y, et al. A distinct class of slow (~0.2-2 Hz) intrinsically bursting layer 5 pyramidal neurons determines UP/DOWN state dynamics in the neocortex. *J Neurosci.* 2015;35:5442-5458.

23. Hughes SW, Cope DW, Blethyn KL, Crunelli V. Cellular mechanisms of the slow (<1Hz) oscillation in thalamocortical neurons *in vitro*. *Neuron.* 2002;33:947-958.

24. Blethyn KL, Hughes SW, Tóth TI, Cope DW, Crunelli V. Neuronal basis of the slow (<1Hz) oscillation in neurons of the nucleus reticularis thalami *in vitro*. *J Neurosci.* 2006;26:2474-2486.

25. Zhu L, Blethyn KL, Cope DW, Tsomaia V, Crunelli V, Hughes SW. Nucleus- and species-specific properties of the slow (<1 Hz) sleep oscillation in thalamocortical neurons. *Neuroscience.* 2006;2006(141):621-636.

26. Crunelli V, Hughes SW. The slow (<1 Hz) sleep rhythm: a dialogue of three cardinal oscillators. *Nat Neurosci.* 2010;13:9-17.

27. O'Reilly C, Iavarone E, Yi J, Hill SL. Rodent somatosensory thalamocortical circuitry: neurons, synapses, and connectivity. *Neurosci Biobehav Rev.* 2021;126:213-235.

28. Meyer HS, Egger R, Guest JM, Foerster R, Reissl S, Oberlaender M. Cellular organization of cortical barrel columns is whisker-specific. *Proc Natl Acad Sci USA.* 2013;110:19113-19118.

29. Meyer HS, Schwarz D, Wimmer VC, et al. Inhibitory interneurons in a cortical column form hot zones of inhibition in layers 2 and 5A. *Proc Natl Acad Sci USA.* 2011;108:16807-16812.

30. Meyer HS, Wimmer VC, Hemberger M, et al. Cell type-specific thalamic innervation in a column of rat vibrissal cortex. *Cereb Cortex.* 2010;20:2287-2303.

31. Oberlaender M, de Kock CP, Bruno RM, et al. Cell type-specific three-dimensional structure of thalamocortical circuits in a column of rat vibrissal cortex. *Cereb Cortex.* 2012;22:2375-2391.

32. Kumar P, Ohana O. Inter- and intralaminar subcircuits of excitatory and inhibitory neurons in layer 6a of the rat barrel cortex. *J Neurophysiol.* 2008;100:1909-1922.

33. Pichon F, Nikonenko I, Kraftsik R, Welker E. Intracortical connectivity of layer VI pyramidal neurons in the somatosensory cortex of normal and barrelless mice. *Eur J Neurosci.* 2012;35:855-869.

34. Petreanu L, Mao T, Sternson SM, Svoboda K. The subcellular organization of neocortical excitatory connections. *Nature.* 2009;457:1142-1145.

35. Lam YW, Sherman SM. Mapping by laser photostimulation of connections between the thalamic reticular and ventral posterior lateral nuclei in the rat. *J Neurophysiol.* 2005;94:2472-2483.

36. Lee CC, Sherman SM. Synaptic properties of thalamic and intracortical inputs to layer 4 of the first- and higher-order cortical areas in the auditory and somatosensory systems. *J Neurophysiol.* 2008;100:317-326.

37. Viaene AN, Petrof I, Sherman SM. Synaptic properties of thalamic input to layers 2/3 and 4 of primary somatosensory and auditory cortices. *J Neurophysiol.* 2011;105:279-292.

38. Sanchez-Vives MV, McCormick DA. Cellular and network mechanisms of rhythmic recurrent activity in neocortex. *Nat Neurosci.* 2000;3:1027-1034.

39. Chagnac-Amitai Y, Luhmann HJ, Prince DA. Burst generating and regular spiking layer 5 pyramidal neurons of rat neocortex have different morphological features. *J Comp Neurol.* 1990;296:598-613.

40. Chagnac-Amitai Y, Connors BW. Synchronized excitation and inhibition driven by intrinsically bursting neurons in neocortex. *J Neurophysiol.* 1989;62:1149-1162.

41. Cauli B, Audinat E, Lambolez B, et al. Molecular and physiological diversity of cortical nonpyramidal cells. *J Neurosci.* 1997;17:3894-3906.

42. Blethyn KL, Hughes SW, Crunelli V. Evidence for electrical synapses between neurons of the nucleus reticularis thalami in the adult brain in vitro. *Thalamus Relat Syst.* 2008;4:13-20.

43. Carnevale NT, Hines ML. *The NEURON Book.* Cambridge University Press; 2006.

44. Sivagnanam S, Majumdar A, Yoshimoto K, et al. Early experience in developing and managing the neuroscience gateway. *Concurr Comput.* 2015;27:473-488.

45. Bédard C, Kröger H, Destexhe A. Modeling extracellular field potentials and the frequency-filtering properties of extracellular space. *Biophys J.* 2004;86:1829-1842.

46. Steriade M, Domich L, Oakson G, Descheˆnes M. The deafferented reticular thalamic nucleus generates spindle rhythmicity. *J Neurophysiol.* 1987;57:260-273.

47. Leresche N, Lightowler S, Soltesz I, Jassik-Gerschenfeld D, Crunelli V. Low-frequency oscillatory activities intrinsic to rat and cat thalamocortical cells. *J Physiol.* 1991;441:155-174.

48. Shu Y, Hasenstaub A, McCormick DA. Turning on and off recurrent balanced cortical activity. *Nature.* 2003;423:288-293.

49. Mann EO, Kohl MM, Paulsen O. Distinct roles of GABA(a) and GABA(B) receptors in balancing and terminating persistent cortical activity. *J Neurosci.* 2009;29:7513-7518.

50. McCafferty C, David F, Venzi M, et al. Cortical drive and thalamic feed-forward inhibition control thalamic output synchrony during absence seizures. *Nat Neurosci.* 2018;21:744-756.

51. David F, Schmiedt JT, Taylor HL, et al. Essential thalamic contribution to slow waves of natural sleep. *J Neurosci.* 2013;33:19599-19610.

52. Steriade M, Contreras D, Curró Dossi R, Nuñez A. The slow (<1 Hz) oscillation in reticular thalamic and thalamocortical neurons: scenario of sleep rhythm generation in interacting thalamic and neocortical networks. *J Neurosci.* 1993;13:3284-3299.

53. Crunelli V, David F, Lőrincz ML, Hughes SW. The thalamocortical network as a single slow wave-generating unit. *Curr Opin Neurobiol.* 2015;31:72-80.

54. Lörincz M, Kekesi K, Juhasz G, Crunelli V, Hughes SW. Temporal framing of thalamic relay-mode firing by phasic inhibition during the alpha rhythm. *Neuron.* 2009;63:683-696.

55. Chauvette S, Volgushev M, Timofeev I. Origin of active states in local neocortical networks during slow sleep oscillation. *Cereb Cortex.* 2010;20:2660-2674.

56. Cossart R, Aronov D, Yuste R. Attractor dynamics of network UP states in the neocortex. *Nature.* 2003;423:283-288.

57. Rudolph M, Pelletier JG, Pare D, Destexhe A. Characterization of synaptic conductances and integrative properties during electrically induced EEG-activated states in neocortical neurons in vivo. *J Neurophysiol.* 2005;94:2805-2821.

58. Haider B, Duque A, Hasenstaub AR, McCormick DA. Neocortical network activity in vivo is generated through a dynamic balance of excitation and inhibition. *J Neurosci.* 2006;26:4535-4545.

59. Schreiner T, Kaufmann E, Noachtar S, Mehrkens JH, Staudigl T. The human thalamus orchestrates neocortical oscillations during NREM sleep. *Nat Commun.* 2022;13(1):5231.

60. Connelly WM, Crunelli V, Errington AC. The global spike: conserved dendritic properties enable unique Ca^{2+} spike generation in low-threshold spiking neurons. *J Neurosci.* 2015;35:15505-15522.

61. Connelly WM, Crunelli V, Errington AC. Passive synaptic normalization and input synchrony-dependent amplification of cortical feedback in Thalamocortical neuron dendrites. *J Neurosci.* 2016;36:3735-3754.

SUPPORTING INFORMATION

Additional supporting information can be found online in the Supporting Information section at the end of this article.